OXFORD

Cerebral Cortex, 2023, **33**, 634–650
https://doi.org/10.1093/cercor/bhac090
Advance access publication date 4 March 2022
Original Article

Neural processes responsible for the translation of sustained nociceptive inputs into subjective pain experience

Hailu Wang[1,2], Yifei Guo[3,4], Yiheng Tu[1,2], Weiwei Peng[5], Xuejing Lu[1,2], Yanzhi Bi[1,2], Gian Domenico Iannetti[3,4], Li Hu[1,2,*]

[1]CAS Key Laboratory of Mental Health, Institute of Psychology, Chinese Academy of Sciences, Beijing 100101, China,
[2]Department of Psychology, University of Chinese Academy of Sciences, Beijing 100049, China,
[3]Neuroscience and Behaviour Laboratory, Istituto Italiano di Tecnologia, Rome 30 16163, Italy,
[4]Department of Neuroscience, Physiology and Pharmacology, University College London, London WC1E 6BT, United Kingdom,
[5]Brain Function and Psychological Science Research Center, Shenzhen University, Shenzhen 518061, China

*Corresponding author: CAS Key Laboratory of Mental Health, Institute of Psychology, Chinese Academy of Sciences, Beijing 100101, China.
Email: huli@psych.ac.cn

Tracking and predicting the temporal structure of nociceptive inputs is crucial to promote survival, as proper and immediate reactions are necessary to avoid actual or potential bodily injury. Neural activities elicited by nociceptive stimuli with different temporal structures have been described, but the neural processes responsible for translating nociception into pain perception are not fully elucidated. To tap into this issue, we recorded electroencephalographic signals from 48 healthy participants receiving thermo-nociceptive stimuli with 3 different durations and 2 different intensities. We observed that pain perception and several brain responses are modulated by stimulus duration and intensity. Crucially, we identified 2 sustained brain responses that were related to the emergence of painful percepts: a low-frequency component (LFC, < 1 Hz) originated from the insula and anterior cingulate cortex, and an alpha-band event-related desynchronization (α-ERD, 8–13 Hz) generated from the sensorimotor cortex. These 2 sustained brain responses were highly coupled, with the α-oscillation amplitude that fluctuated with the LFC phase. Furthermore, the translation of stimulus duration into pain perception was serially mediated by α-ERD and LFC. The present study reveals how brain responses elicited by nociceptive stimulation reflect the complex processes occurring during the translation of nociceptive information into pain perception.

Key words: nociceptive information; pain perception; alpha-band oscillations; phase-amplitude coupling; mediation effects.

Introduction

In a dynamic environment, the temporal structures of sensory events evolve at multiple temporal scales, extending from transient to sustained periods (Werner and Noppeney 2011; Palva and Palva 2018). The human brain has evolved to track and predict the temporal structures of such events and thereby produce appropriate actions (Panzeri et al. 2010). When considering nociceptive stimuli, this function is critical to ensure survival, as appropriate and immediate reactions are necessary to avoid actual or potential bodily injury (Moayedi et al. 2015; Mouraux and Iannetti 2018).

The neural processes triggered by transient nociceptive stimuli have been extensively studied. These stimuli elicit a series of brain responses in human electroencephalogram (EEG) (Mouraux and Iannetti 2009; Hu, Valentini, et al. 2014; Ploner et al. 2017), dominated by a large, negative–positive biphasic vertex wave (Garcia-Larrea et al. 2003; Treede et al. 2003). The amplitude of the vertex wave strongly depends on the saliency of the transient nociceptive stimulus, i.e. on how much the stimulus contrasts with neighboring sensory inputs in either time or space (Downar et al. 2000; Iannetti et al. 2008; Legrain et al. 2011). Saliency detection is considered a key attentional mechanism that promotes survival by enabling individuals to focus their limited perceptual and cognitive resources on the most behaviorally relevant information (Corbetta and Shulman 2002; Kayser et al. 2005). However, the vertex wave is not able to track the temporal structures of tonic nociceptive stimuli: for example, long-lasting and not fast-rising nociceptive inputs do not elicit a vertex wave (Ploner et al. 2017; Mouraux and Iannetti 2018; Somervail et al. 2021).

To address the issue of the neural correlate of sustained nociceptive input, a growing number of

Received: November 2, 2021. **Revised:** January 24, 2022. **Accepted:** February 11, 2022

studies investigated the neural responses elicited by sustained nociceptive stimuli (Peng et al. 2014; Schulz et al. 2015; Colon et al. 2017; Nickel et al. 2020). These studies demonstrated that neural responses different from the transient vertex wave encode the temporal dynamics of nociceptive inputs by distinct neural responses (Zhang et al. 2016; Nickel et al. 2017; Guo et al. 2020; Mulders et al. 2020). For example, fluctuations of sustained nociceptive inputs are reflected by the centro-parietal modulations of alpha (α) and beta (β) oscillations, which likely originate from the sensorimotor cortex (Nir et al. 2012; Peng et al. 2014). Moreover, the temporal dynamics of sustained and periodic nociceptive inputs could also be encoded by low-frequency component (LFC; e.g. <1 Hz) of brain responses originating from the insula and anterior cingulate cortex (Colon et al. 2017; Liberati et al. 2019; Mulders et al. 2020).

Although neural responses elicited by sustained nociceptive stimuli (especially for periodic stimuli) are being investigated, the neural processes responsible for translating sustained nociceptive information into subjective pain perception are not yet fully elucidated. To tap into this issue, it is necessary to characterize and compare pain perception and brain responses to nociceptive stimuli by varying stimulus characteristics, such as their intensity and duration (Mulders et al. 2020).

Therefore, this exploratory study aimed to investigate (i) whether and how pain perception and neural responses encode stimulus duration and intensity, (ii) how the encoded neural responses interact when tracking the temporal structures of nociceptive inputs, and (iii) whether the measured neural responses mediate the relationship between nociceptive stimulation and the ensuing pain perception. To address these questions, we recorded 64-channel EEG from 48 healthy participants receiving sustained and nonperiodic thermo-nociceptive stimuli with 3 durations and 2 intensities. Both LFC (<1 Hz) and neural oscillations in α and β frequencies (8–13 Hz and 20–22 Hz, respectively) were extracted and compared between different experimental conditions. The relationship between these brain responses at different frequencies was assessed using phase–amplitude coupling (PAC), and their neural origin was estimated using source analysis. The causal relationship between characteristics of nociceptive stimulation, the resulting neural responses and pain perception was modeled using multilevel mediation analysis.

Materials and methods

Subjects

Forty-eight healthy right-handed subjects (24 females), aged 24.5 ± 3.2 years (mean $\pm$ SD, range = 20–35 years), participated in the study. None reported acute pain at the time of examination or a history of chronic pain. All subjects were given their written informed consent before the experiment and were paid for their participation. The local ethics committee approved the experimental procedures.

Nociceptive stimulation and experimental design

Noxious contact heat stimuli were generated by a thermode (CHEPs, Medoc Ltd, Ramat Yishai, Israel) with a circular contact area of 572.5 mm^2 (27 mm diameter). The temperature at the thermode surface was increased at a rate of 70 °C/s using a thermofoil, and decreased at a rate of 40 °C/s using a Peltier device. The baseline temperature at the thermode surface was 42 °C, and the target temperature was individually determined before data collection and computer-controlled. A pair of thermocouples under the thermode surface provided a continuous measure of the temperature at the skin–thermode interface at a sampling rate of 150 Hz. During the experiment, the thermode was fixed to the left volar forearm by an elastic Velcro strap provided by the equipment. The position of the thermode was kept constant throughout each block and was slightly changed in different blocks to minimize nociceptor sensitization or habituation.

The experimental design is shown in Fig. 1. A total of 6 stimulation types (3 stimulus durations × 2 stimulus intensities) were included in the experiment. For each stimulation type, the contact heat stimulus was composed of 3 phases (Fig. 1): the temperature increased from baseline (42 °C) to target (t1 or t2) with a speed of 70 °C/s; the temperature remained constant for 0.5 s (D1), 1 s (D2), or 2 s (D3); the temperature decreased from target to baseline with a speed of 40 °C/s. The target temperature (t1 or t2), which could evoke a pain rating of 5 (I1) or 7 (I2) on the 0–10 numerical rating scale (NRS, where 0 is "no pain" and 10 is "pain as bad as it could be"), was individually determined before the formal experiment. Specifically, the target temperature was determined using the ascending method of limits: increasing the target temperature (initially set at 45 °C) in steps of 0.5 °C, until a rating of 5 or 7 was obtained on the 0–10 NRS. Such procedures were repeated 3 times, and the average temperature was used as the target temperature for each stimulation type and subject. As such, the target temperature for each stimulation intensity and each subject would be different, and the target temperature would be identical for different stimulus durations of the same stimulus intensity.

The formal experiment consisted of 6 blocks, and in each block, 30 contact heat stimuli (5 stimuli for each stimulation type) were delivered. In total, there were 180 trials for each subject and 30 trials for each stimulation type. The interstimulus interval (ISI) varied randomly from 12 to 16 s. Trials with different stimulation types were delivered pseudorandomly to ensure no more than 2 consecutive stimuli of the same stimulation type in the trial sequence. Three seconds after the offset of each stimulus, subjects were instructed to rate the highest perceived pain on the same 0–10 NRS.

EEG data collection and preprocessing

Subjects were seated in a comfortable chair in a silent, temperature-controlled room. They were instructed

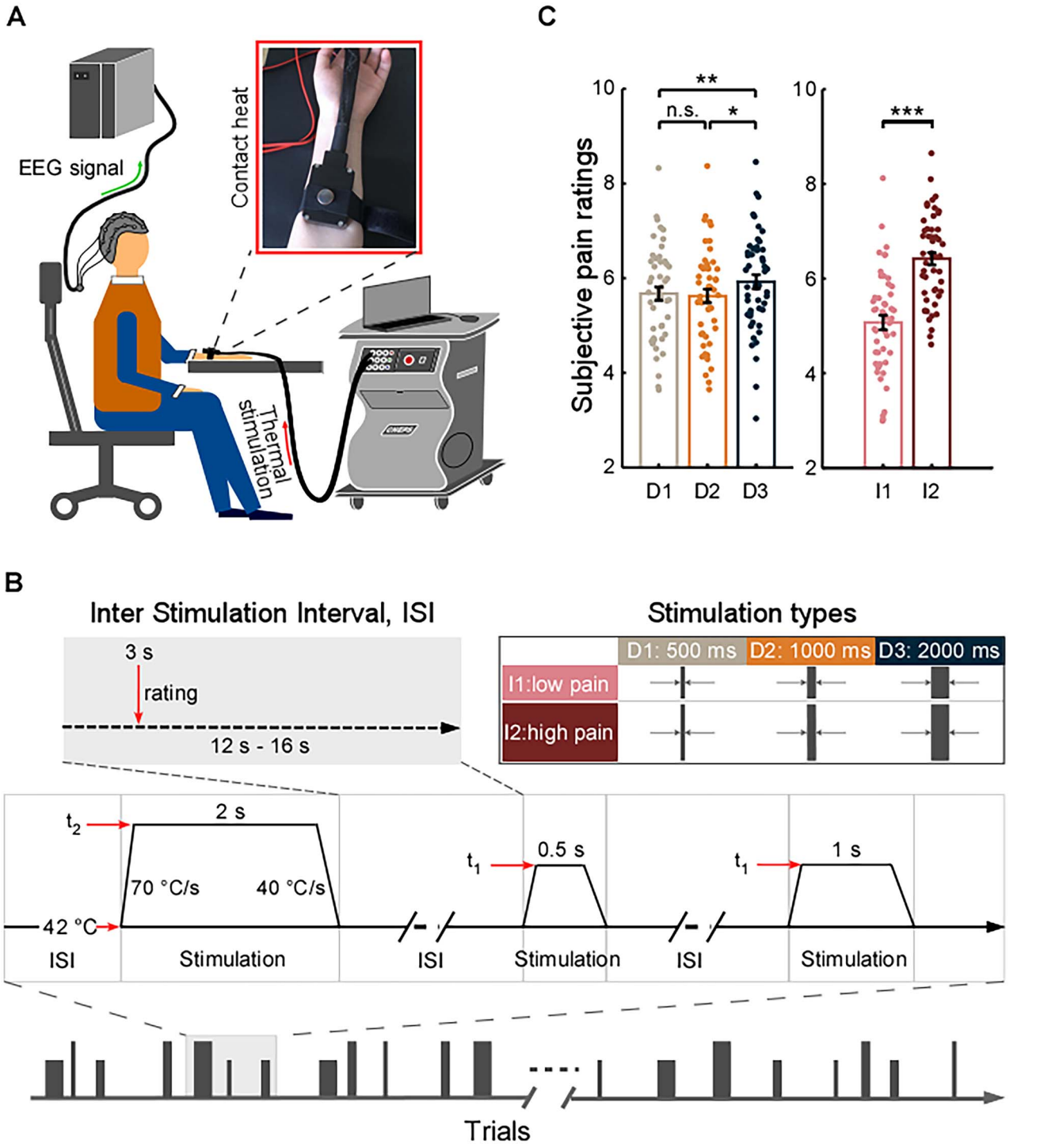

Fig. 1. Experimental design and behavioral results. (A) Experimental setup. Participants were seated comfortably with their left forearm resting on a table in front of them. Cutaneous nociceptive afferents of the left volar forearm were stimulated using fast-rising contact heat (Peltier thermode, 27 mm diameter), while 64-channel EEG was simultaneously collected. (B) Experimental design. A total of 6 stimulation types (3 durations × 2 intensities) were included in the experiment. Each contact heat stimulus consisted of 3 phases: A temperature increase from baseline (42°C) to target (t1 or t2), with a speed of 70°C/s; a plateau of constant temperature lasting 500, 1,000, or 2,000 ms; and a temperature decrease from target to baseline, with a speed of 40°C/s. the target temperature (t1 or t2) was individually determined in a preliminary experiment to obtain a pain rating of 5 or 7 on a 0–10 NRS. Three seconds after each stimulus, subjects were instructed to rate the highest perceived pain on the same 0–10 NRS. The ISI varied randomly from 12 to 16 s. The 6 stimulus types were delivered pseudorandomly. (C) Behavioral results. Pain ratings for stimuli of different durations and intensities are shown in the left and right panels, respectively. Pain ratings elicited by contact heat of longer duration (i.e. D3) were higher than shorter durations (i.e. D1 and D2). Moreover, pain ratings elicited by contract heat of high intensity (i.e. I2) were higher than that of low intensity (i.e. I1). Error bars represent the standard error of the mean (SEM). *: $P < 0.05$; **: $P < 0.01$; ***: $P < 0.001$.

to focus their attention on the stimuli, relax their muscles, keep their eyes open, and gaze slightly downward. The EEG data were recorded using 64 Ag–AgCl scalp electrodes placed according to the international 10–20 system (Brain Products GmbH, Munich, Germany; passband: 0.01–100 Hz; sampling rate: 1000 Hz). The left mastoid (M1) was used as the online reference, and all electrode impedances were kept lower than 10 kΩ. To monitor ocular movements and eye blinks, electrooculographic signals were simultaneously recorded from 2 surface electrodes: 1 placed over the left lower eyelid, and the other placed ~10 mm lateral to the outer canthus of the left orbit.

EEG data were preprocessed using EEGLAB (Delorme and Makeig 2004), an open-source toolbox running under the MATLAB environment. EEG epochs were extracted using a window analysis time of 5,000 ms (1,000 ms before and 4,000 ms after stimulus onset), and baseline corrected using the prestimulus interval. Trials contaminated by eye blinks and movements were corrected using an independent component analysis algorithm (runica in EEGLAB). In all datasets, independent components with a large electrooculographic electrode contribution and a frontal scalp distribution were removed. In total, there were 4.7 ± 3.1 (mean ± SD) components removed with the ICA. After preprocessing, EEG epochs were rereferenced to the common average.

Contact heat evoked potentials

To extract the typical contact heat evoked potentials (CHEP) waveforms, preprocessed EEG data were bandpass filtered between 1 and 30 Hz, and baseline corrected using the prestimulus interval. For each subject and stimulation type, single-trial CHEP waveforms in the time domain were averaged together. Peak latencies and amplitudes of N2 and P2 waves, defined as the most negative and positive deflections between 150 and 500 ms after stimulus onset, respectively, were measured from each single-subject average waveform, at Cz (average reference). Single-subject average CHEP waveforms were subsequently averaged across subjects for each stimulation type to obtain group-level CHEP waveforms. Group-level scalp topographies at the peak latency of N2 and P2 waves were computed by spline interpolation.

Low-frequency component

To extract LFC evoked by contact heat, preprocessed EEG data were low-pass filtered at 1 Hz, and baseline corrected using the prestimulus interval. For each subject and stimulation type, single-trial LFC waveforms in the time domain were averaged together. The response durations and amplitudes of LFC were measured from each single-subject average waveform. According to the scalp distribution of the LFC, a positive LFC was measured from the central-parietal region (i.e. Cz and Pz), and a negative LFC was measured from bilateral frontal-temporal regions (i.e. FT7 and FT8). The response duration of LFC was calculated as the time length of positive or negative response beyond the threshold (i.e. 2 standard deviations of the prestimulus interval for each single-subject average waveform) within the poststimulus onset interval (i.e. 0–4,000 ms) for positive and negative LFC, respectively. The response amplitude of LFC was calculated by averaging the positive or negative response within the above-defined LFC response duration for positive and negative LFC, respectively. Single-subject average LFC waveforms were subsequently averaged across subjects for each stimulation type to obtain group-level LFC waveforms. Group-level scalp topographies of LFC within the poststimulus onset interval (i.e. 0–3,000 ms, in which the LFC was presented) were computed by spline interpolation.

Time-frequency analysis

In addition to the above phase-locked brain responses, a time-frequency analysis was performed to explore the nonphase-locked brain responses elicited by contact heat stimuli (e.g. event-related desynchronization at the alpha frequency, α-ERD) (Pfurtscheller and Lopes da Silva 1999; Hu and Iannetti 2019). Time–frequency distributions (TFDs) of single-trial EEG signals were estimated using a windowed Fourier transform (WFT) with a fixed 0.3-s Hanning window. The WFT yielded, for each single trial, a complex time–frequency estimate $F(t, f)$ at each point (t, f) in the time–frequency plane, extending from −1 to 4 s (in steps of 1 ms) in the time domain, and from 1 to 100 Hz (in steps of 1 Hz) in the frequency domain. The resulting spectrogram, $P(t,f) = |F(t, f)|$, represents the signal magnitude as a joint function of time and frequency at each time–frequency point. The spectrograms were log-transformed and then baseline-corrected (reference interval: −0.8 to −0.2 s relative to stimulus onset) at each frequency using the subtraction approach (Hu, Xiao, et al. 2014; Hu and Zhang 2019).

According to previous studies (Nir et al. 2012; Peng et al. 2014), fluctuations of sustained nociceptive stimuli could be encoded by the centro-parietal modulations of alpha (α) and beta (β) oscillations, i.e. α-ERD and β-ERD. Within their respective frequency range (8–13 Hz for α-ERD and 20–22 Hz for β-ERD), we estimated the time course of signal amplitude by averaging the amplitude across all included frequencies. Afterward, we estimated the response durations and amplitudes of the time–frequency features for each stimulation type and subject using the same method described in the LFC analysis.

Source analysis

Source analyses were performed using the Brain Electrical Source Analysis software (BESA 5.3, https://www.besa.de/). To estimate the locations of LFC, distributed source analysis based on Classical LORETA (Pascual-Marqui et al. 1994) Analysis Recursively Applied (Classical LORETA Analysis Recursively Applied – CLARA) (Hoechstetter et al. 2010) was performed on group-level average LFC waveforms. CLARA was achieved by performing a weighted LORETA with a reduced source space at each iteration. As compared to LORETA

(Pascual-Marqui et al. 1994), this iterative approach reduces the blurring of the estimated sources while keeping the advantage of a predefined distributed source model, thus making it easier to determine the location of the source with maximal activity (Hoechstetter et al. 2010; Hamalainen et al. 2011). The locations and strengths of LFC sources were obtained for a 1,500-ms long interval (500–2,000 ms within the poststimulus onset interval) corresponding to the largest part of the LFC responses.

To estimate the locations of α-ERD, Multiple Source Beamformer, a modified version of the linearly constrained minimum variance vector beamformer in the time–frequency domain (Gross et al. 2001; Kurimoto et al. 2008), was performed on single-trial EEG waveforms. A beamformer operator is designed to pass signals from the brain region of interest without attenuation while minimizing interference from activity in all other brain regions (Jonmohamadi et al. 2014; Nunes et al. 2020). As compared to the traditional Single Source Beamformer that mislocalizes sources if several brain regions are highly correlated (Michel et al. 2004; Nunes et al. 2020), Multiple Source Beamformer contains the leadfields of the source at the region of interest and possibly interfering sources at other regions, thus providing a more accurate estimation of sources (Nunes et al. 2020). The locations and strengths of the α-ERD sources were obtained within the poststimulus onset time–frequency region (500–2000 ms, 8–13 Hz) corresponding to the largest part of the response. Since scalp topographies of LFC and α-ERD were similar for all stimulus conditions (Supplementary Figs S1 and S2), source analyses were performed on all EEG data regardless of stimulus conditions to improve the accuracy of source estimation. For both LFC and α-ERD sources, locations were finally transformed to Talairach space.

Phase–amplitude coupling

Alpha oscillations occurring at different phases of the low-frequency oscillations between distinct brain regions are proposed to be associated with interbrain area communications (Purdon et al. 2013). To assess whether α-oscillations and LFC were coupled, cross-frequency PAC was calculated between α-ERD at C4 (where α-ERD was maximal) and LFC at all other electrodes (since LFC was widespread distributed) using PAC. The strength of PAC was estimated using the envelope-to-signal correlation method (Bruns and Eckhorn 2004; Onslow et al. 2011), which was achieved using the following procedures. First, single-trial EEG data at C4 were band-pass filtered between 8 and 13 Hz to calculate α-oscillations (S_α). Second, S_α was analyzed using the Hilbert transform to estimate the signal envelope, $Amp_\alpha = Abs\ (Hilbert(S_\alpha))$. Third, single-trial EEG data at other electrodes were low-pass filtered at 1 Hz and demeaned to calculate LFC (S_{LF}). Finally, the Pearson correlation between Amp_α and S_{LF} was computed for each single trial (Bruns and Eckhorn 2004; Vanneste et al. 2018). To test whether the strength of PAC was significantly different from the chance level, we performed a permutation test (1,000 times) by randomly shuffling the trial numbers of Amp_α and S_{LF} and comparing the group-level PAC strength and its corresponding null distribution generated by 1,000 random permutations. Moreover, to assess the possible time lag between α-oscillations and LFC, the cross-correlation between Amp_α and S_{LF} was also computed for each single trial with the lag of one signal over the other ranging from −1,000 to 1,000 ms. The time lag at which cross-correlation coefficients peaked was considered to represent the temporal difference between the 2 signals with maximal coupling.

To assess whether the coupling between α-oscillations and LFC was associated with contact heat stimulation, the PAC analysis was repeatedly performed on EEG signals within both prestimulus and poststimulus onset intervals (−4,000 to 0 ms and 0–4,000 ms for prestimulus and poststimulus onset intervals, respectively). Note that EEG signals from −4,000 to 4,000 ms relative to stimulus onset were processed using the same procedures as the signals mentioned above (i.e. −1,000 to 4,000 ms relative to stimulus onset).

To provide a detailed exploration of the cross-frequency coupling, we also quantified the relationship between the envelope of α-oscillations and the phase of LFC using the following procedures. First, we extracted the instantaneous phase of LFC ($Phase_{LF}$ = angle (Hilbert (S_{LF}))) within the poststimulus onset interval for each trial, and equally divided $Phase_{LF}$ into 10 bins from $-\pi$ to π (each bin covers 36°). Then, we pooled all envelope amplitudes of α-oscillations to the corresponding phase bins, and calculated the average amplitude of α-oscillations in each bin. Finally, to eliminate the effect of scale difference between subjects, we normalized the amplitude of α-oscillations by (i) log-transforming the data to ensure normal distribution and (ii) converting the transformed data to Z scores. The PAC between α-oscillations and LFC was presented using both bar plots and radar maps, before and after phase bin shifting, which provided better visualization of the matching between the 2 signals.

Multilevel mediation analysis

To reveal how the brain translates different characteristics (i.e. stimulus duration and intensity) in contact heat into the intensity of pain perception, we performed 2-path and 3-path multilevel mediation analyses using the Multilevel Mediation and Moderation (M3) Toolbox (Wager et al. 2008). In the 2-path mediation models, stimulus duration and stimulus intensity were respectively used as the independent variables (X). Subjective ratings of pain perception were the dependent variable (Y). The extracted brain features, including the latency and amplitude of N2 and P2 waves, response duration and amplitude of LFC and α-ERD, were the mediator (M). The same as described in Tiemann et al. (2018), 5 path coefficients were calculated for each subject in

each 2-path mediation model, and the path coefficients quantified the relationship from X to M (path a), the relationship from M to Y controlled for X (path b), the relationship from X to Y (path c), the relationship from X to Y controlled for M (path c′), and the mediation effect (path a*b). In the multilevel mediation analysis, the group-level path coefficients were estimated by averaging weighted single-subject path coefficients, and the weights for each subject were determined based on a weighted least squares-based mixed-effects model taking within- and between-subject variance into account (Tiemann et al. 2018). The group-level mediation effects were calculated by multiplying coefficients of path a and path b and adding the covariance of path a and path b (Wager et al. 2008).

In the 3-path mediation models, stimulus duration and stimulus intensity were respectively used as the independent variables (X). Subjective ratings of pain perception were the dependent variable (Y). Any pair of the extracted brain features were used as the 2 mediators (M1 and M2). Six path coefficients were calculated for each subject in each 3-path mediation model, and the path coefficients quantified the relationship from X to M1 (path a), the relationship from M1 to M2 controlled for X (path d), the relationship from M2 to Y controlled for M1 (path b), the relationship from X to Y (path c), the relationship from X to Y controlled for M1 and M2 (path c′), and the mediation effect (path a*d*b).

It should be noted that (i) the signal-to-noise ratio of single-trial EEG responses was meager, and (ii) brain responses in every single trial were modulated by the combined effects of stimulus duration and intensity due to the within-subject experimental design. To separately explore the mediation effects from the 2 stimulus characteristics of nociceptive inputs to the intensity of pain perception, it would be necessary to assemble single trials before performing the mediation analyses to eliminate the possible influence of the interaction effect between the 2 stimulus characteristics. Specifically, when considering stimulus duration as the independent variable, we randomly extracted 20% trials with identical stimulus intensities for each stimulus duration (i.e. D1, D2, and D3). The data of the extracted trials were averaged to ensure that (i) the signal-to-noise ratio of the extracted brain responses was higher, (ii) the extracted brain responses were not influenced by stimulus intensity, and (iii) the within-subject variability of brain responses across different stimulus durations was preserved. The same assembling trials procedure was also applied when considering stimulus intensity as the independent variable.

Statistical analyses

To test whether stimulus characteristics had an effect on perceptual and electrophysiological responses elicited by contact heat, we performed a 2-way repeated-measures analysis of variance (ANOVA) with "stimulus duration" (D1, D2, and D3) and "stimulus intensity" (I1 and I2) as within-subject factors. Post hoc paired-sample *t*-tests were performed when the interaction between the 2 factors was significant. To highlight the respective effect of stimulus duration and stimulus intensity on perceptual and electrophysiological responses elicited by contact heat, post hoc paired-sample *t*-tests were also performed when the main effect was significant. To account for multiple comparisons in the analyses, a false discovery rate (FDR) procedure (Benjamini and Hochberg 1995) was adopted to adjust the *P* values.

Results

Subjective pain perception

Single-trial ratings of pain perception were clearly dependent on both stimulus duration and stimulus intensity (Fig. 1C). As summarized in Supplementary Tables S1 and S2, 2-way repeated-measures ANOVA showed strong evidence for main effects of "stimulus duration" ($F_{(2, 94)} = 7.05$, $P = 0.001$, Partial $\eta^2 = 0.13$) and "stimulus intensity" ($F_{(1, 47)} = 249.3$, $P < 0.001$, Partial $\eta^2 = 0.84$). There was also strong evidence for a significant interaction between the 2 factors ($F_{(2, 94)} = 15.03$, $P < 0.001$, Partial $\eta^2 = 0.24$). Post hoc paired-sample *t*-tests showed that for all stimulus durations (i.e. D1, D2, and D3), there was strong evidence that pain perception elicited by contact heat of high stimulus intensity (I2) was higher than that of low stimulus intensity (I1) (all $P < 0.001$). For high stimulus intensity (I2), there was moderate-to-strong evidence that pain perception elicited by contact heat of longer duration (D3) was higher than that of shorter durations (D1, $P < 0.001$; and D2, $P = 0.001$). However, for lower stimulus intensity (I1), no significant difference was observed between longer duration (D3) and shorter durations (D1, $P = 0.8$ and D2, $P = 0.99$). Moreover, no significant difference was observed between D1 and D2 for both stimulus intensities ($P = 0.99$ for I1; $P = 0.68$ for I2).

Contact heat evoked potentials

Group-level CHEP waveforms and scalp topographies of N2 and P2 waves, which are the typical vertex waves that have been described in the Introduction, are shown in Fig. 2A. As summarized in Supplementary Table S1, N2 and P2 waves were maximal at approximately 230 and 360 ms after stimulus onset, respectively. While the scalp topography of the N2 wave was maximal at the vertex and extended bilaterally towards temporal regions, the scalp topography of the P2 wave was more centrally distributed.

Results of the 2-way repeated measures ANOVA are summarized in Supplementary Table S2. As expected, for both N2 and P2 amplitudes, there was moderate-to-strong evidence for a main effect of "stimulus intensity" (N2: $F_{(1, 47)} = 11.8$, $P = 0.001$, Partial $\eta^2 = 0.2$; P2: $F_{(1, 47)} = 6.37$, $P = 0.015$, Partial $\eta^2 = 0.12$), indicating that N2 and P2 amplitudes were larger when the

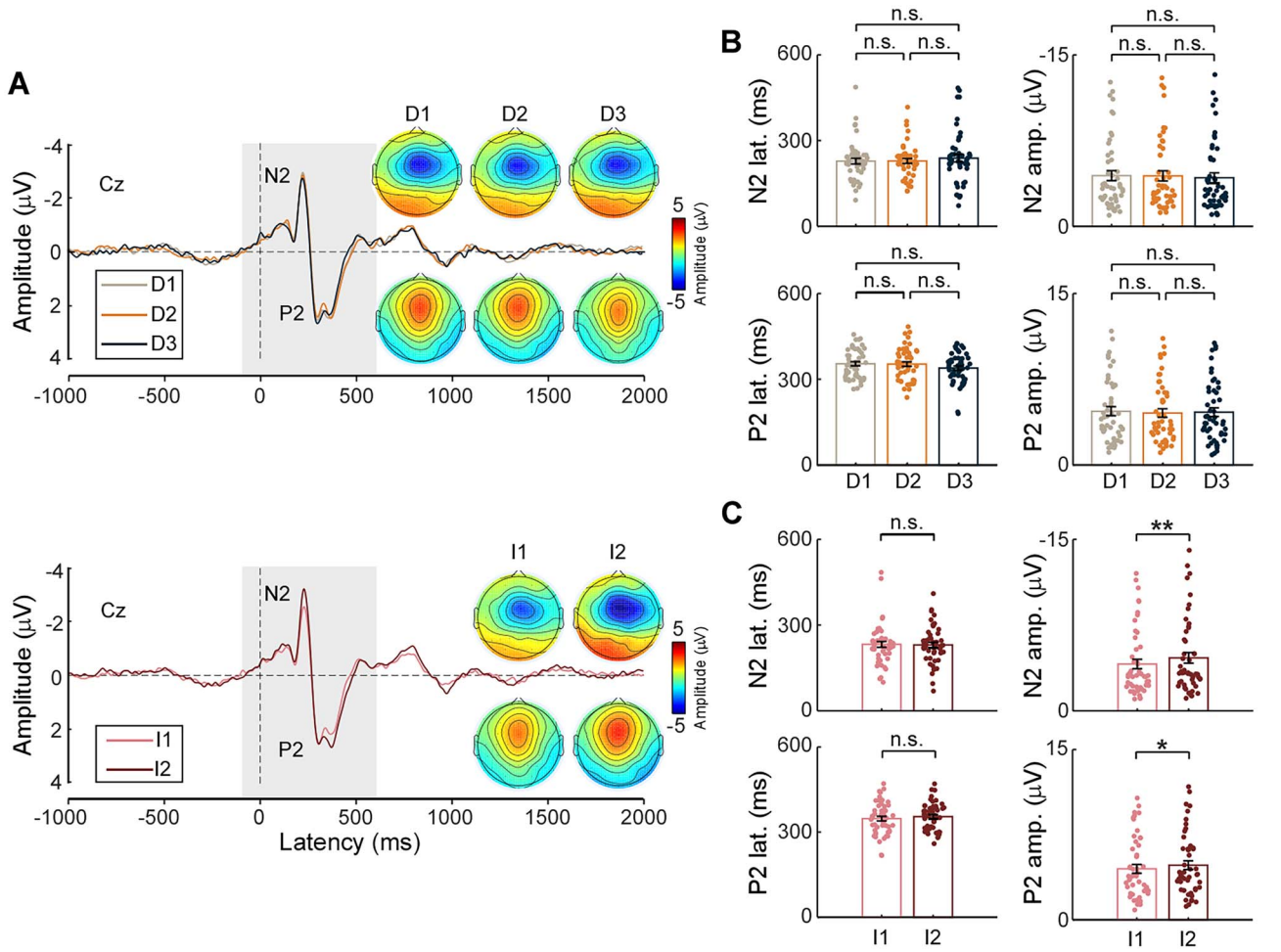

Fig. 2. Brain potentials (CHEPs, 1–30 Hz) evoked by contact heat stimulation. (A) Group-level waveforms and scalp topographies of contact heat-evoked potentials. The EEG data were collected from 64 electrodes in 48 subjects. Displayed waveforms were recorded from the vertex (Cz, average reference), and color-coded according to stimulus duration (D1, D2, and D3) and intensity (I1 and I2). Scalp topographies are displayed at the peak latency of the main negative (N2) and positive (P2) waves. (B, C) Comparisons of N2 and P2 latencies and amplitudes at different stimulus durations and intensities. Error bar represents SEM. n.s.: not significant; *: $P < 0.05$; **: $P < 0.01$.

stimulus intensity was higher (Fig. 2C). However, there was no significant main effect of "stimulus duration" and interaction between the 2 factors for both N2 and P2 amplitudes (Supplementary Table S2 and Fig. 2B). Moreover, no significant main effects of "stimulus duration" and "stimulus intensity," as well as their interaction, were observed for N2 and P2 latencies (Supplementary Table S2, Fig. 2B and C). These results confirm that the vertex waves elicited by fast-rising nociceptive stimuli reflect the differential increase of stimulus intensity at stimulus onset, but not the duration of the plateau at target intensity (see Fig. 2 in Somervail et al. 2021).

Low-frequency component

To examine whether brain responses at low frequencies (i.e. 0.01–1 Hz) (Colon et al. 2017; Liberati et al. 2019; Mulders et al. 2020) could encode stimulus duration and intensity, we extracted the time-domain LFC by low-pass filtering at 1 Hz, following the online high-pass filtering at 0.01 Hz. Group-level waveforms and scalp topographies of LFC are shown in Fig. 3. In all stimulus conditions, there was a clear positive LFC maximal at the central-parietal region and a negative LFC maximal at bilateral frontal–temporal regions. Interestingly, the scalp topographies of LFC were stable for the entire duration of the response across all stimulus conditions (Supplementary Fig. S1).

Duration and amplitude of the LFC at some representative electrodes (i.e. Cz, Pz, FT7, and FT8) are summarized in Supplementary Table S3, and results of the 2-way repeated measures ANOVA are summarized in Supplementary Table S4.

LFC duration

There was weak evidence for a main effect of "stimulus duration" on the duration of the positive LFC measured at Cz ($F_{(2, 94)} = 4.36$, $P = 0.015$, Partial $\eta^2 = 0.085$). Post hoc paired-sample *t*-tests revealed that a longer stimulus duration evoked a longer LFC (e.g. D1 vs. D3; $P = 0.019$). Moreover, there was moderate-to-strong evidence for a

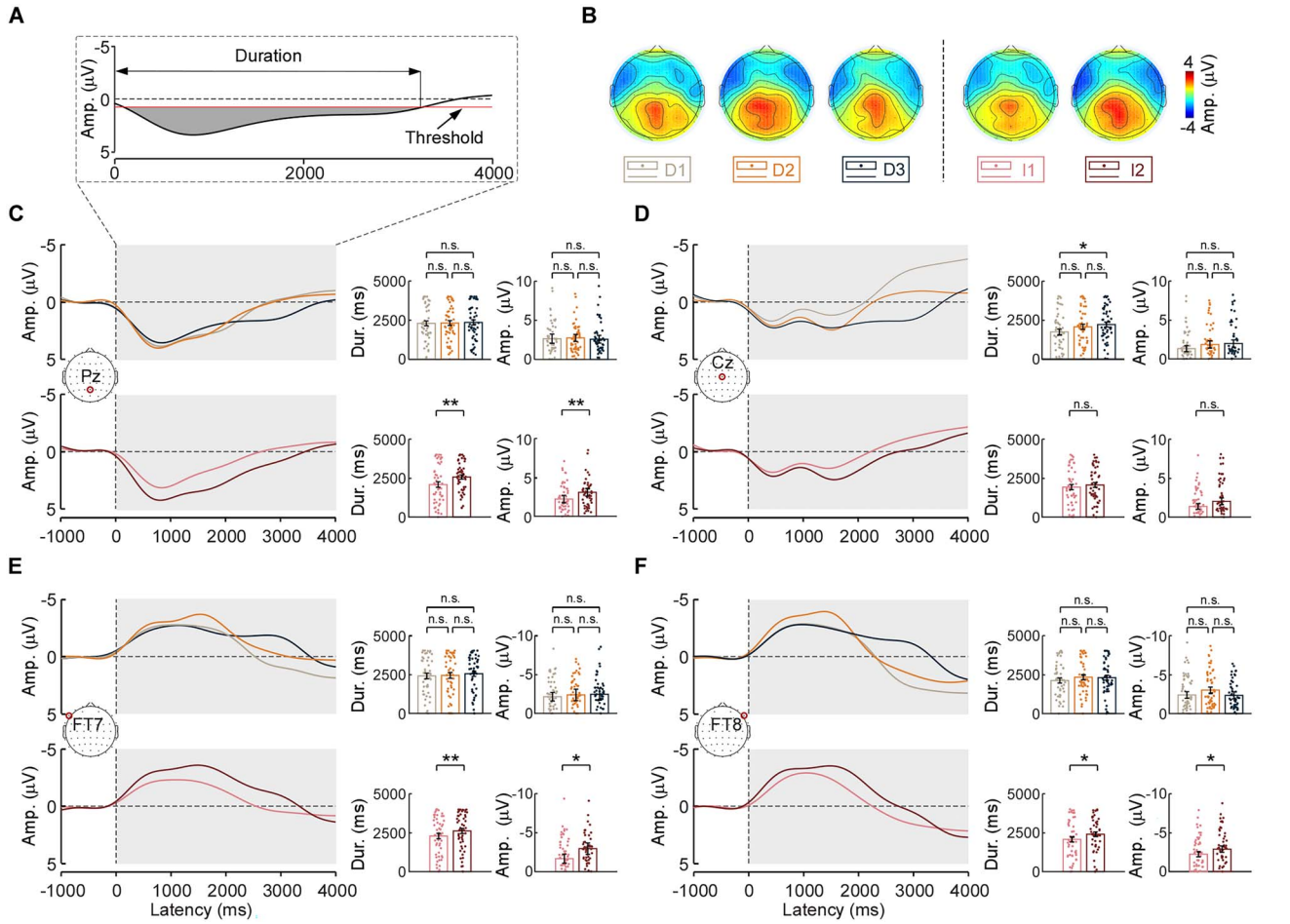

Fig. 3. The LFC (0.01–1 Hz) evoked by contact heat stimulation. (A) The schematic diagram illustrates the method to extract the LFC response duration, taking the positive response as an example. The threshold was defined as 2 standard deviations of EEG signals within the prestimulus onset interval for each single-subject average waveform. The response duration of LFC was calculated as the time length of positive or negative response beyond the threshold within the poststimulus onset interval (i.e. 0–4,000 ms) for positive and negative LFC, respectively. (B) Scalp topographies of LFC are displayed for each condition by calculating the mean amplitude of LFC within the poststimulus onset interval (0–3,000 ms). (C, D, E, and F) Time courses of LFC evoked by contact heat stimulation. Displayed waveforms were recorded from Pz, Cz, FT7, and FT8 (average reference), respectively, and color-coded according to stimulus durations (D1, D2, and D3, top left in each panel) and intensities (I1 and I2, bottom left in each panel). The comparisons of LFC durations and amplitudes at different stimulus durations and different stimulus intensities are shown in the right part of each panel. Error bar represents SEM. n.s.: not significant; *: $P < 0.05$; **: $P < 0.01$.

main effect of "stimulus intensity" on positive LFC duration at Pz ($F_{(1, 47)} = 11.5$, $P = 0.001$, Partial $\eta^2 = 0.19$) and on negative LFC duration at FT7 ($F_{(1, 47)} = 7.9$, $P = 0.007$, Partial $\eta^2 = 0.14$) and FT8 ($F_{(1, 47)} = 6.07$, $P = 0.017$, Partial $\eta^2 = 0.11$). Post hoc paired-sample *t*-tests revealed that a higher stimulus intensity also evoked a longer LFC, regardless of positive or negative, than a lower stimulus intensity (i.e. I1 vs. I2, $P = 0.001$ for Pz; $P = 0.007$ for FT7; $P = 0.017$ for FT8). No significant interaction between the 2 factors was observed for both positive and negative LFC durations (Supplementary Table S4).

LFC amplitude

There was weak-to-moderate evidence for a main effect of "stimulus intensity" on the amplitude of positive LFC measured at Pz ($F_{(1, 47)} = 10.4$, $P = 0.002$, Partial $\eta^2 = 0.18$) and of negative LFC measured at FT7 ($F_{(1, 47)} = 6.24$, $P = 0.016$, Partial $\eta^2 = 0.12$) and FT8 ($F_{(1, 47)} = 6.23$, $P = 0.016$, Partial $\eta^2 = 0.11$). Post hoc paired-sample *t*-tests revealed that a higher stimulus intensity evoked a LFC of larger amplitude (either positive or negative) than a lower stimulus intensity (i.e. I1 vs. I2, $P = 0.002$ for Pz; $P = 0.016$ for FT7; $P = 0.016$ for FT8). In contrast, there was no evidence of either a main effect of "stimulus duration" or an interaction between the 2 factors (Supplementary Table S4).

Stimulus-induced modulations of neural oscillations

Next, we examined whether stimulus-induced modulations of neural oscillations, which we estimated using the time–frequency analysis, also encoded the duration and intensity of the eliciting stimulus. Group-level TFDs, together with the scalp topographies of event-related desynchronization at α (α-ERD) and β (β-ERD) frequencies, are shown in Fig. 4A and C. Consistently with previous studies (Mouraux et al. 2003;

Baumgartner et al. 2012; De Schoenmacker et al. 2021), nociceptive stimuli elicited not only large phase-locked responses (100–500 ms, 1–10 Hz) corresponding to the N2 and P2 vertex waves in the time domain but also clear nonphase-locked responses (α-ERD: 8–13 Hz, β-ERD: 20–22 Hz). Please note that α-ERD and β-ERD were similarly maximal at the contralateral central region and submaximal at the ipsilateral central region for all stimulus conditions, and the scalp topographies of both responses were highly consistent from its onset to offset (Supplementary Fig. S2).

The response duration and amplitude of α-ERD and β-ERD at C4 are summarized in Supplementary Table S5, and the results of the 2-way repeated measures ANOVA are summarized in Supplementary Table S6.

α-ERD duration

There was strong evidence for a main effect of "stimulus duration" ($F_{(2, 94)} = 13.12$, $P < 0.001$, Partial $\eta^2 = 0.218$) and weak evidence for a main effect of "stimulus intensity" ($F_{(1, 47)} = 6.23$, $P = 0.016$, Partial $\eta^2 = 0.12$) on α-ERD duration. No significant interaction between the 2 factors was observed (Supplementary Table S6). Post hoc paired-sample t-tests showed that there was strong evidence that α-ERD duration was longer in the D3 condition than in D1 ($P < 0.001$) and D2 ($P = 0.001$) conditions, while no difference was observed between D1 and D2 conditions ($P = 0.99$). Moreover, there was weak evidence that α-ERD duration was longer for the I2 condition than the I1 condition ($P = 0.016$).

α-ERD amplitude

There was strong evidence for a main effect of "stimulus duration" ($F_{(2, 94)} = 12.3$, $P < 0.001$, Partial $\eta^2 = 0.21$) and weak evidence for a main effect of "stimulus intensity" ($F_{(1, 47)} = 6.24$, $P = 0.016$, Partial $\eta^2 = 0.12$) on α-ERD amplitude. No significant interaction between the 2 factors was observed (Supplementary Table S6). Post hoc paired-sample t-tests showed moderate-to-strong evidence that α-ERD amplitude was larger in the D3 condition than in D1 ($P < 0.001$) and D2 ($P = 0.002$) conditions, while no difference was observed between D1 and D2 conditions ($P = 0.99$). Moreover, there was weak evidence that α-ERD amplitude was larger for the I2 condition than the I1 condition ($P = 0.016$).

β-ERD duration

There was moderate evidence for the main effect of "stimulus duration" ($F_{(2, 94)} = 5.5$, $P = 0.005$, Partial $\eta^2 = 0.106$) on β-ERD duration. No significant main effect of "stimulus intensity" and interaction between the 2 factors was observed (Supplementary Table S6). Post hoc paired-sample t-tests showed that β-ERD duration was significantly longer for the D3 condition than the D2 condition ($P = 0.015$), while no significant difference was observed between D1 and D2 conditions as well as between D1 and D3 conditions. Moreover, β-ERD duration was not significantly different between I2 and I1 conditions ($P = 0.8$).

β-ERD amplitude

There was moderate evidence for the main effect of "stimulus duration" ($F_{(2, 94)} = 5.97$, $P = 0.003$, Partial $\eta^2 = 0.11$) on β-ERD amplitude. No significant main effect of "stimulus intensity" and interaction between the 2 factors was observed (Supplementary Table S6). Post hoc paired-sample t-tests showed that β-ERD amplitude was significantly larger for the D3 condition than the D2 condition ($P = 0.01$), while no significant difference was observed between D1 and D2 conditions as well as D1 and D3 conditions. Moreover, β-ERD amplitude was not significantly different between I2 and I1 conditions ($P = 0.9$). Due to the similarity in features and functions between α-ERD and β-ERD and the relatively higher signal-to-noise ratio of α-ERD than β-ERD (Jeon et al. 2011), we focused on describing α-ERD results in the following sections.

LFC and α-ERD sources

To estimate the neural origins of both LFC and α-ERD elicited by contact heat stimuli, we performed source analyses using CLARA (Hoechstetter et al. 2010) and Multiple Source Beamformer (Gross et al. 2001; Kurimoto et al. 2008), respectively. As shown in Fig. 5A, LFC sources were located in the insula contralateral (Talairach coordinates: 31.5, −23.9, 9.7 mm; maximal intensity: 1.29 nAm/cm^3) and ipsilateral (Talairach coordinates: −38.5, −9.9, 2.7 mm; maximal intensity: 1.38 nAm/cm^3) to the stimulated side, as well as in the anterior cingulate cortex (Talairach coordinates: −10.5, 32.1, 9.7; maximal intensity: 0.78 nAm/cm^3). As displayed in Fig. 5B, α-ERD sources were located in the primary sensorimotor cortex contralateral (Talairach coordinates: 31.5, −16.9, 51.7 mm; maximal intensity: −16.98%) and ipsilateral (Talairach coordinates: −24.5, −23.9, 51.7 mm; maximal intensity: −6.43%) to the stimulated side.

Phase–amplitude coupling

To assess the relationship between the LFC and α-ERD, we calculated the cross-frequency coupling between the phase of LFC and the amplitude of α-oscillations (PAC; Fig. 6A and B). Relative to α-amplitude measured at C4, positive coupling was observed for the phase of LFC at bilateral frontal–temporal electrodes (e.g. FT7 and FT8), and negative coupling was observed at parietal electrodes (e.g. P3 and P4). The permutation test demonstrated that the strength of PAC, either positive or negative, was significantly larger than the chance level at these scalp locations (Fig. 6B). Interestingly, the largest PACs were observed when the LFC phases were shifted by a certain degree (−72° for both positive and negative couplings, Fig. 6D). When examining the temporal relationship between the LFC phase and α-amplitude using cross-correlation analysis, the fluctuation of

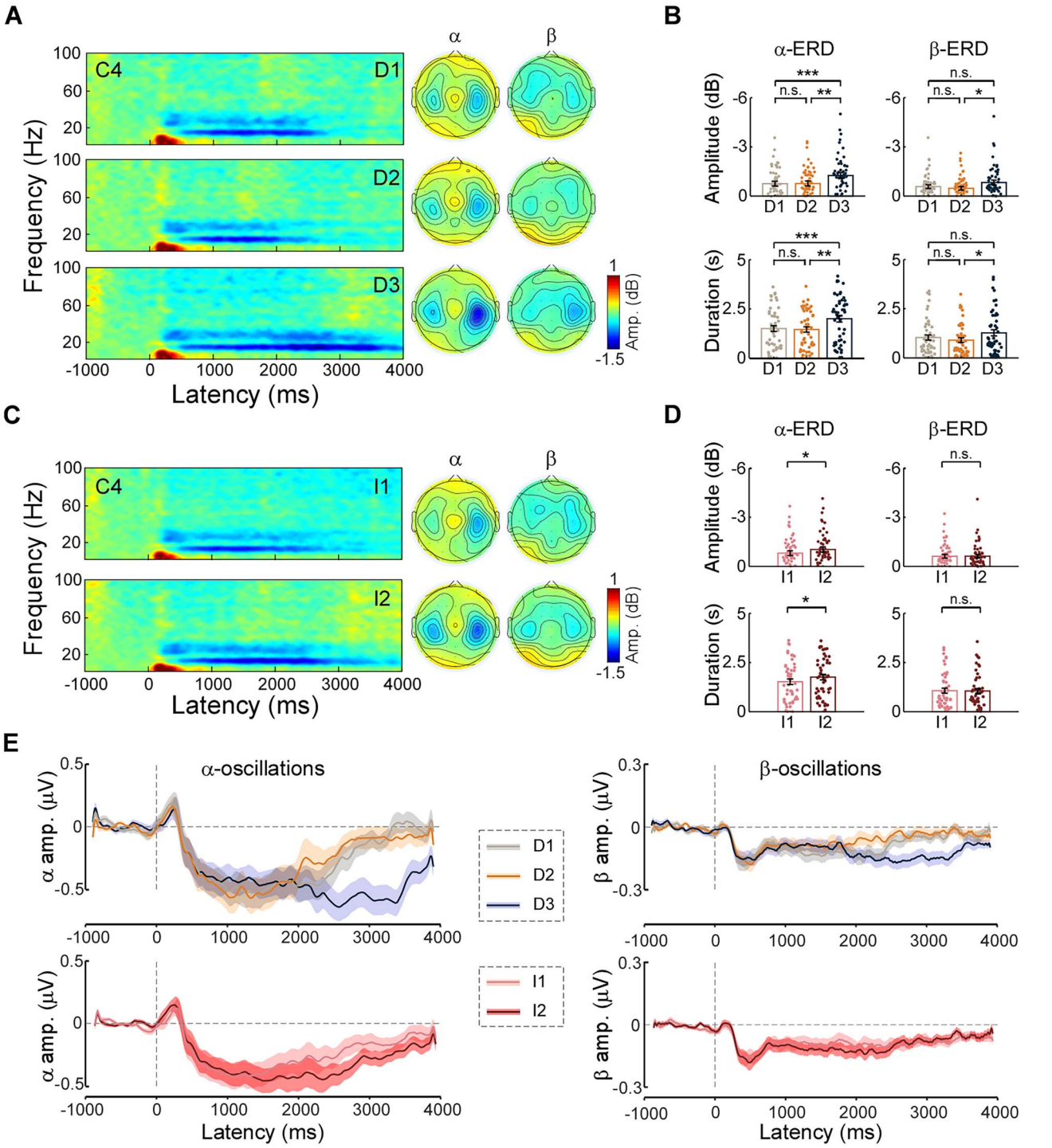

Fig. 4. Event-related modulations of neural oscillations elicited by contact heat stimulation. (A, C) TFDs elicited by contact heat stimulation of different durations (D1, D2, and D3; A left) and intensities (I1 and I2; C left). Scalp topographies of α-ERD (8–13 Hz, 0–4 s) and β-ERD (20–22 Hz, 0–4 s) are displayed for each stimulus duration (A right) and intensity (C right). (B, D) Comparisons of α-ERD and β-ERD duration and amplitude at different stimulus durations and intensities. Error bar represents SEM. n.s.: not significant; *: $P < 0.05$; **: $P < 0.01$; ***: $P < 0.001$. (E) The time courses of α-ERD (left) and β-ERD (right) at different stimulus durations (top) and intensities (bottom).

α-amplitude was maximally coupled to the LFC phase with a fixed time lag: specifically, it was by approximately 170–230 ms for positive coupling (when LFC phases were measured at FT7 and FT8), and by approximately 170–200 ms for negative coupling (when LFC phases were measured at P3 and P4) (Supplementary Fig. S3).

The PAC strength in different experimental conditions is summarized in Supplementary Table S7 and Fig. 6C, and results of the 2-way repeated measures ANOVA are summarized in Supplementary Table S8. For the positive PAC observed on the left hemisphere (LFC phase was extracted from Cluster 1, i.e. F7, FT7, and FC5), there was moderate evidence for the main effect of "stimulus

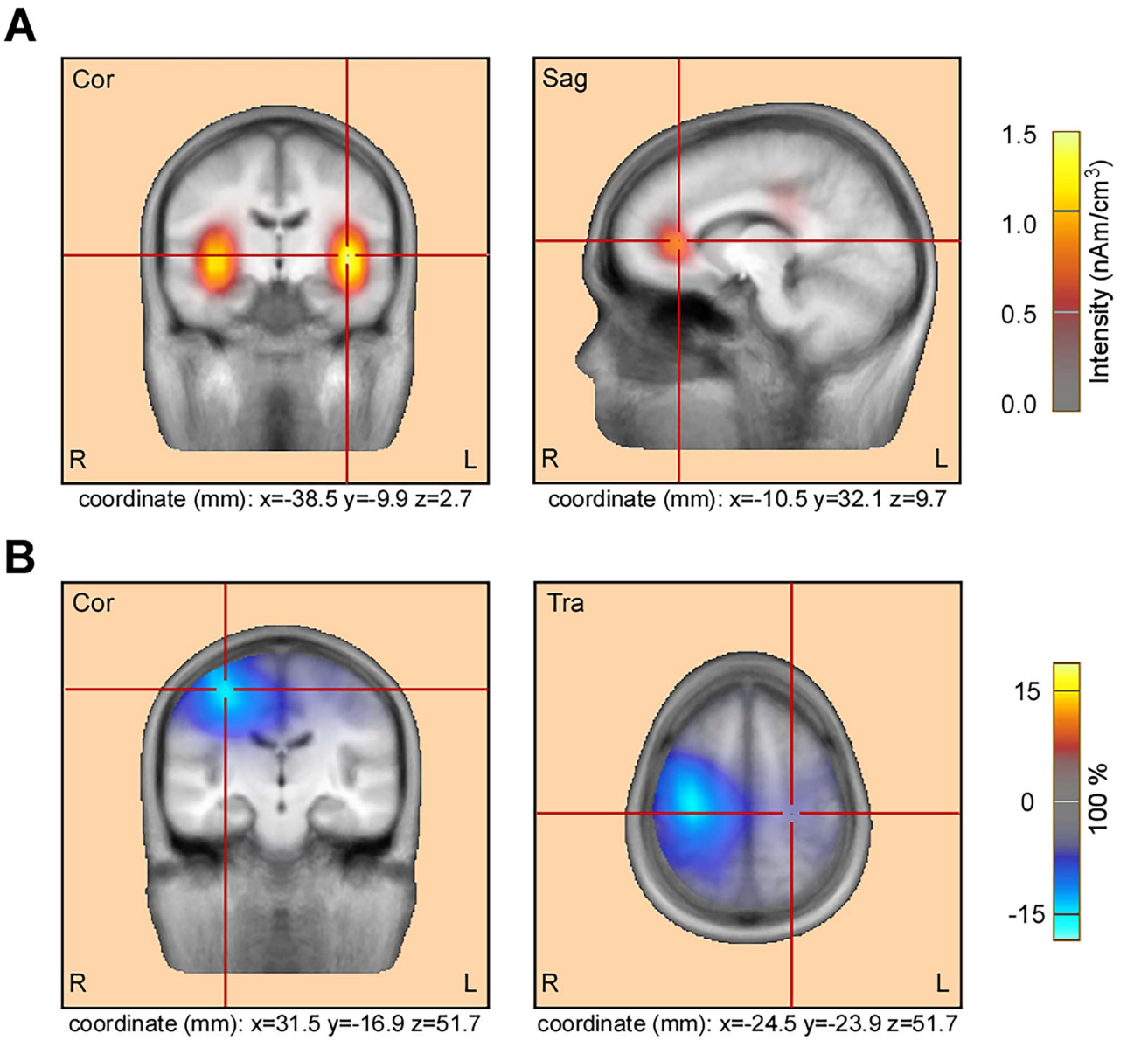

Fig. 5. Distributed sources of LFC and α-ERD elicited by contact heat stimulation. (A) Distributed sources of LFC were estimated using CLARA, superimposed on standard MR image template, and color-coded according to their intensities, expressed in nAm/cm^3. LFC sources were located in bilateral insula (Talairach coordinates: 31.5, −23.9, 9.7 mm and −38.5, −9.9, 2.7 mm; maximal intensity: 1.29 and 1.38 nAm/cm^3) and anterior cingulate cortex (Talairach coordinates: −10.5, 32.1, 9.7; maximal intensity: 0.78 nAm/cm^3). (B) Distributed sources of α-ERD were estimated using multiple source beamformer, superimposed on a standard MR image template, and color-coded according to their intensities, expressed in percentage of elicited power relative to baseline power (from −800 to −200 ms). α-ERD sources were located in the contralateral S1 (Talairach coordinates: 31.5, −16.9, 51.7 mm; maximal intensity: −16.98%) and ipsilateral S1 (Talairach coordinates: −24.5, −23.9, 51.7 mm; maximal intensity: −6.43%).

intensity" ($F_{(1, 47)} = 9.88$, $P = 0.003$, FDR corrected, Partial $\eta^2 = 0.17$), but no evidence for the main effect of "stimulus duration" and interaction between the 2 factors (Supplementary Table S8). For the positive PAC observed on the right hemisphere (LFC phase was extracted from Cluster 2, i.e. F8, FT8, and FC6) and negative PAC (LFC phase was extracted from Cluster 3, i.e. CP1, CPz, CP2, P3, P1, Pz, P2, P4, and POz), there was no evidence for main effects of "stimulus duration" and "stimulus intensity," as well as for their interaction (Supplementary Table S8). These results indicated that PAC was partly modulated by stimulus intensity: a stronger PAC was induced by a higher stimulus intensity in Cluster 1. In contrast, the PAC strength was equally large (significantly larger than the chance level) for all stimulus durations.

Notably, PAC strength estimated from EEG signals within the prestimulus onset interval was also significantly larger than the chance level for both positive and negative couplings (Supplementary Fig. S4). However, PAC strength was significantly larger for EEG signals within the poststimulus onset interval than the pre-stimulus onset interval ($P < 0.05$ for FT7 and P3; Supplementary Fig. S4).

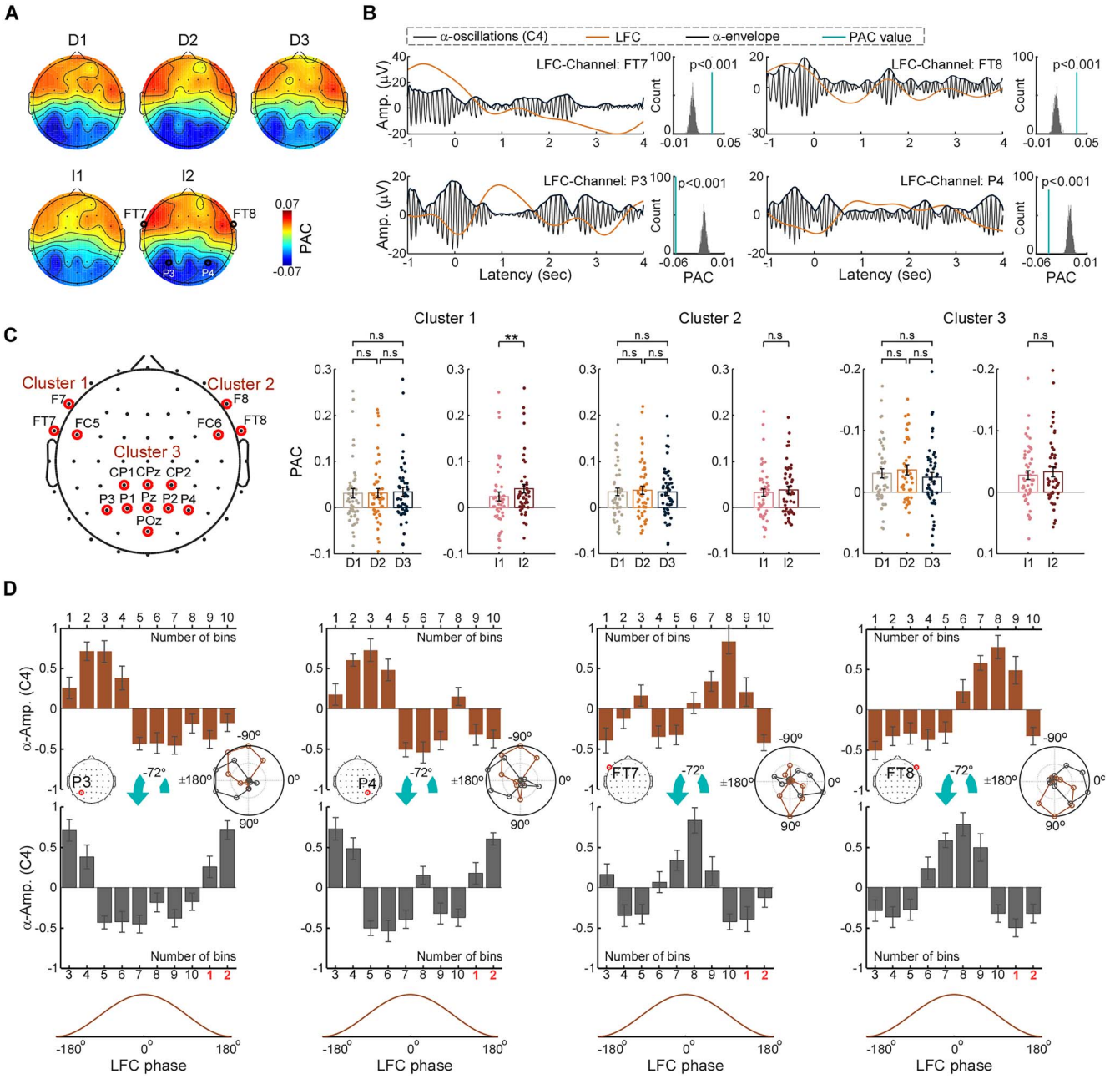

Fig. 6. Cross-frequency coupling between the phase of the LFC and the amplitude of α-oscillations. (A) Scalp topographies of PAC between LFC phase and α-amplitude at different stimulus durations (top) and different stimulus intensities (bottom). Please note that the α-amplitude was always measured from C4, where the α-ERD response was dominantly observed, and the LFC phase was extracted from all electrodes to calculate PAC scalp topographies. (B) Representative trials showing different patterns of PAC from four electrodes and their group-level statistical results. Positive coupling was observed between LFC phases at FT7 and FT8 and α-amplitudes at C4 (top); negative coupling was observed between LFC phases at P3 and P4 and α-amplitudes at C4 (bottom). Permutation tests indicated that the PAC at the demonstrated electrodes was significantly stronger than chance level. (C) The comparison of PACs at different stimulus durations and different stimulus intensities. The PACs were estimated when LFC phases were extracted from electrodes at 3 different clusters (cluster 1: F7, FT7, and FC5; cluster 2: F8, FT8, and FC6; cluster 3: CP1, CPz, CP2, P3, P1, Pz, P2, P4, and POz). Error bar represents SEM. n.s.: not significant; **: $P < 0.01$. (**D**) The detailed relationship between LFC phases and α-amplitudes. LFC phases were grouped into 10 bins, and the corresponding α-amplitudes (represented as z values) were calculated to demonstrate their coupling. For both positive (LFC phases were measured at FT7 and FT8) and negative (LFC phases were measured at P3 and P4) couplings, the largest PACs were observed when the LFC phases were shifted by a certain degree (approximately −72° or 2 bins). The radar maps show the effects of phase shifting, and the error bar represents SEM across subjects.

Mediation effects of different brain responses

We adopted multilevel mediation analyses to assess whether neural responses mediate the relationship between characteristics of nociceptive stimulation (duration and intensity) and the ensuing pain perception. Supplementary Tables S9 and S10 showed all 2-path coefficients for the mediation analyses when stimulus duration and stimulus intensity were respectively used as independent variables. Specifically, the α-ERD duration significantly mediated the effect of stimulus duration on subjective pain ratings ($\beta_{ab} = 0.08$, $P = 0.02$, FDR corrected, Fig. 7B), and the N2 and P2 amplitudes

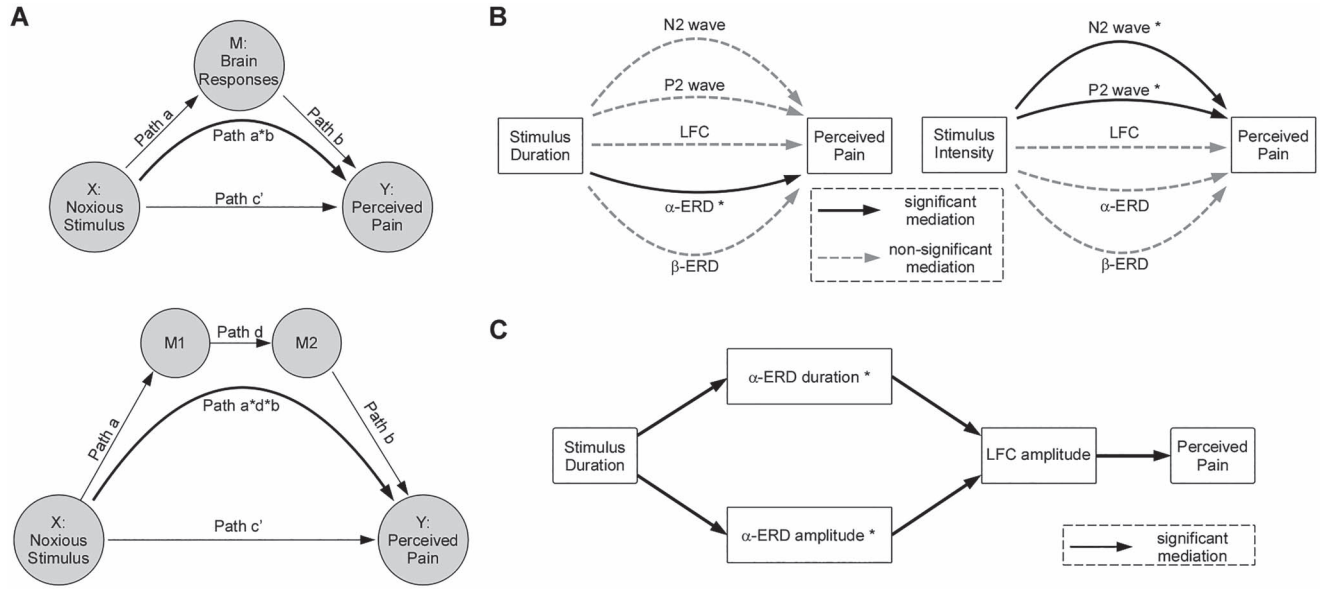

Fig. 7. Two-path and 3-path mediation analyses. (A) The schematic diagrams of 2-path (top) and 3-path (bottom) mediation models in mediation analyses. For the 2-path mediator, path *a* represents the relation of X (noxious stimulus) to M (a brain response), path *b* represents the relation of M to Y (perceived pain) controlled for X, and path *c'* is the relation of X to Y controlled for M. mediation effects are calculated by multiplying coefficients of path *a* and path *b* and tested for significance using a bootstrap approach. For the 3-path mediator, path *a* represents the relation of X (noxious stimulus) to M1 (a brain response), path *d* represents the relation of M1 to M2 (another brain response) controlled for X, path *b* represents the relation of M2 to Y (perceived pain) controlled for M1, and path *c'* is the relation of X to Y controlled for M1 and M2. Mediation effects are calculated by multiplying coefficients of path *a*, path *d*, and path *b* and tested for significance using a bootstrap approach. (B) Left panel shows, for 2-path mediation analysis, the mediation effect of brain responses on the relationship between stimulus duration and perceived pain. The duration of α-ERD significantly mediated the effect of stimulus duration on subjective ratings of perceived pain ($\beta_{ab} = 0.08$, $P = 0.02$, FDR corrected). The right panel represents the mediation effect of brain responses on the relationship between stimulus intensity and perceived pain. Amplitudes of N2 and P2 waves significantly mediated the effect of stimulus intensity on subjective ratings of perceived pain (N2: $\beta_{ab} = 0.01$, $P = 0.02$, FDR corrected; P2: $\beta_{ab} = 0.01$, $P = 0.03$, FDR corrected). (C) Three-path mediator analysis revealed the mediation effect of brain responses on the relationship between stimulus duration and perceived pain. The duration of α-ERD (M1) and the amplitude of LFC (M2) serially mediated the effect of stimulus duration on subjective ratings of perceived pain ($\beta_{adb} = 0.001$, $P = 0.01$, FDR corrected). Moreover, the amplitude of α-ERD (M1) and the amplitude of LFC (M2) serially mediated the effect of stimulus duration on subjective ratings of perceived pain ($\beta_{adb} = 0.001$, $P = 0.009$, FDR corrected).

significantly mediated the effect of stimulus intensity on subjective pain ratings (N2: $\beta_{ab} = 0.01$, $P = 0.02$, FDR corrected; P2: $\beta_{ab} = 0.01$, $P = 0.03$, FDR corrected, Fig. 7B).

Supplementary Table S11 showed all 3-path coefficients for the mediation analyses when stimulus duration was used as the independent variable. Specifically, the α-ERD duration (M1) and the LFC amplitude (M2) serially mediated the effect of stimulus duration on subjective pain ratings ($\beta_{adb} = 0.001$, $P = 0.01$, FDR corrected, Fig. 7C). Moreover, the α-ERD amplitude (M1) and the LFC amplitude (M2) serially mediated the effect of stimulus duration on subjective pain ratings ($\beta_{adb} = 0.001$, $P = 0.009$, FDR corrected, Fig. 7C). No significant 3-path mediation effect of brain responses on the relationship between stimulus intensity and perceived pain was observed.

Discussion

In this study, we aimed to understand the neural processing responsible for the transition of sustained nociceptive information into subjective pain experience. We delivered noxious contact heat with 3 stimulus durations and 2 stimulus intensities and measured both the transient brain responses (e.g. the N2–P2 vertex waves) associated with the onset of nociceptive stimuli and the sustained brain responses (e.g. the LFC and α-ERD) related to the tonic part of nociceptive stimuli as well as pain perception. Our results revealed how brain responses could reflect the complex processes occurring during the transformation of sustained nociceptive information into the subjective pain experience.

Brain responses elicited by transient nociceptive stimuli

Thanks to the high temporal resolution of the EEG technique, we were able to tease out brain responses elicited by the onset of nociceptive stimulation from those consequent to the sustained nociceptive stimulation. The potential elicited by stimulus onset displayed its typical biphasic N2-P2 complex maximal at the scalp vertex (Fig. 2). This vertex potential can be elicited by stimuli of virtually all sensory modalities provided that they are salient (Downar et al. 2000; Iannetti et al. 2008; Legrain et al. 2011) and largely reflect supramodal neural activity that is not specific to nociceptive inputs, but highly associated with stimulus salience (Mouraux and Iannetti 2009; Hu, Cai, et al. 2014). A longstanding misconception in pain neurophysiology is that the vertex potential is able to capture information about the neural activity giving rise to pain perception. This has been consequent to the fact that the vertex potential is often correlated

to pain perception given the frequent but not obligatory coupling between stimulus intensity and stimulus salience (Mouraux and Iannetti 2009; Legrain et al. 2011). However, this coupling can be effectively disrupted, thus demonstrating that the vertex potential does not provide information about nociceptive activity leading to pain perception, and, particularly about the long-lasting temporal dynamics of nociceptive inputs, e.g. stimulus duration (Fig. 2).

Brain responses elicited by sustained nociceptive stimuli

Brain activities reflecting the more tonic part of nociceptive stimulation were mostly 2: the LFC generated in the bilateral insula and ACC and the α-ERD generated from the sensorimotor cortex (Figs 3–5). The β-ERD had a timecourse similar to that of the α-ERD. These observations are in line with previous observations (Peng et al. 2014; Nickel et al. 2017; Ploner et al. 2017; Guo et al. 2020; Mulders et al. 2020), showing that neural responses at different frequencies (e.g. α- and β-frequencies) encode the temporal dynamics of the stimulus. A novel finding of this study is that sustained and nonperiodic noxious stimuli not only induced a nonphase-locked modulation of ongoing sensorimotor α- and β-oscillations (Nickel et al. 2017; Mulders et al. 2020), but also evoked a phase-locked brain response at lower frequencies (i.e. <1 Hz) in the ACC and/or the operculo-insular cortices (Colon et al. 2017; Liberati et al. 2019; Mulders et al. 2020). Moreover, our findings extend those of previous studies showing that α-ERD and LFC encoded stimulus intensity (Peng et al. 2014; Mulders et al. 2020) by demonstrating that both LFC and α-ERD were also sensitive to stimulus duration (Figs 3 and 4).

It is noteworthy that significant differences of LFC and α-ERD parameters, as well as subjective ratings of pain perception, were observed between D1 (0.5 s) and D3 (2 s) conditions as well as between D2 (1 s) and D3 (2 s) conditions, but not between D1 and D2 conditions (Figs 3 and 4). This discrepancy could be associated with the nature of these sustained brain responses, given that they were elicited by slowly- adapting thermonociceptors that gradually respond to contact heat (Colon et al. 2017; Mulders et al. 2020), or, more likely, due to an inherent lack of temporal precision of contact heat in both the intensity and the timing of activation of free nerve endings at nociceptor depth. Indeed, although the temporal profile of the temperature can be reliably controlled at the thermode surface, the temperature at the nociceptor level is not only lower but also delayed, since subcutaneous tissue acts as a heat sink—a problem that becomes worse with high heating rise times (Tillman et al. 1995; Magerl and Treede 1996). This caveat likely explains why the time course of both LFC and α-ERD responses showed a maximal response approximately from 1 to 2 s for both D1 and D2 conditions, and from 1 to 3 s for D3 condition, after the onset of nociceptive stimuli (Figs 3 and 4).

Importantly, we observed significant cross-frequency coupling between the phase of LFC and the amplitude of α-oscillations, and the largest PAC was observed when the LFC phase was shifted by a certain degree (Fig. 6). This cross-frequency coupling was also observed in spontaneous EEG activity within the prestimulus onset interval, although this coupling was relatively weaker than in the poststimulus onset EEG activity (Supplementary Fig. S4). Please note that source analyses suggested that the α-ERD was originated from the sensorimotor cortex (i.e. the lateral pain system), and the LFC was generated from bilateral insula and ACC (i.e. the medial pain system). The PAC between the LFC and α-oscillations might suggest an ongoing communication, even in the absence of nociceptive inputs, between the structures composing the lateral and medial pain systems (Albe-Fessard et al. 1985; Dong et al. 1994; Treede et al. 1999).

Mediation effects

Beyond the typical bivariate analyses to assess the relationship between stimulus inputs and pain perception and/or brain responses, multilevel mediation analyses could quantify how brain responses mediate the relationship between nociceptive information and subjective experience of pain perception, thus providing some mechanistic insights into the stimulus–brain–behavior relationships (Tiemann et al. 2018). When stimulus intensity was used as the independent variable in the current study, we observed that amplitudes of N2 and P2 waves significantly mediated the effect of stimulus intensity on pain perception (Fig. 7B). This observation is in line with recent EEG and functional magnetic resonance imaging studies (Atlas et al. 2014; Woo et al. 2015; Tiemann et al. 2018) and suggests that N2 and P2 waves are functionally involved in the translation of stimulus intensity into pain perception. Since N2 and P2 waves reflect stimulus salience (Legrain et al. 2011) and there is a close relationship between stimulus intensity and salience in the current experimental design (Iannetti and Mouraux 2010), the present finding could reflect the influence of stimulus salience on perceptual processes via N2 and P2 waves.

When stimulus duration was used as the independent variable, we observed that the duration and amplitude of α-ERD (M1) and the amplitude of LFC (M2) serially mediated the effect of stimulus duration on pain perception (Fig. 7C). This observation not only verified that both α-ERD and LFC are important neural responses in encoding stimulus duration (Figs 3 and 4) but also indicated that the coupling between the 2 brain responses might be crucial for the conversion of sustained nociceptive information into pain perception (Fig. 6). Since α-ERD and LFC were generated from brain regions in the lateral and medial pain systems, respectively (Fig. 5), the serial mediation effect would imply that the conversation from stimulus duration to pain perception involves serial neural processing of multiple brain regions/systems. Notably,

the serial neural processing was in line with the cortical hierarchy in the nociceptive system to encode the temporal dynamics of nociceptive inputs (Treede et al. 1999; Tracey and Mantyh 2007), i.e. from α-ERD that was originated from the sensorimotor cortex (the low-level brain regions) to LFC that was generated from bilateral insula and ACC (the high-level brain regions).

Limitations, future directions, and conclusions

The main caveat of the current study is that although we used 3 stimulus durations of nominally 500, 1,000, and 2,000 ms, it is unlikely that they resulted in similar durations at the physiologically meaningful level of nociceptive afferents (Baumgartner et al. 2005)—as we have detailed earlier in the Discussion. For this reason, the lack of difference between D1 and D2 should be taken with a pinch of salt, as it is possible that D1 and D2 did not differ by 500 ms. This lack of precision obviously affected less the difference between D1/D2 vs. D3, since the nominal temperature at the Peltier surface in D3 was 1.5 or 1 s longer than D1 and D2, respectively.

Previous studies suggested that gamma oscillations (30–100 Hz) in the medial prefrontal cortex also encoded the fluctuations of nociceptive input and resulting pain perception (Schulz et al. 2015; Nickel et al. 2017). In our study, after increasing the signal-to-noise ratio by averaging signal amplitude across all gamma frequencies, we found moderate evidence that the gamma amplitude was significantly modulated by "stimulus intensity" ($F_{(1, 47)} = 7.8$, $P = 0.007$, Partial $\eta^2 = 0.14$), but not by "stimulus duration," and there was no interaction between the 2 factors. Due to the inherently low signal-to-noise ratio of EEG oscillations at higher frequencies (e.g. gamma and beta oscillations) and the limited spatial resolution of EEG signals measured at the scalp level, solid conclusions can only be made in future studies with either higher density scalp recordings from a large number of subjects or intracranial recordings from patients or animal models.

Previously, the LFC was shown to be preferentially elicited by nociceptive somatosensory inputs compared to auditory stimuli of similar intensity (Guo et al. 2020). This finding, along with the fact that sustained nociceptive inputs are not as salient as transient stimuli, would indicate that our observations related to stimulus duration were not associated with the general stimulus saliency. Moreover, α-ERD showed a maximal distribution at the contralateral central region and was demonstrated to be originated from the sensorimotor cortex, which suggested the somatosensory-selective nature of the response as compared with α-ERD induced by auditory and visual stimuli (Romei et al. 2008; Hu et al. 2013). However, since we did not use a control condition in a different sensory modality, it is unknown whether the coupling between LFC and α-ERD that we observed is pain-selective. Therefore, future studies should be performed to evaluate their coupling in other sensory modalities using carefully matched stimulus intensity.

In summary, the present study provides novel evidence for ongoing communications between the lateral and medial pain systems, thus shedding new light on the importance of the interplay of neural responses at different frequencies in different brain regions for the generation of pain perception. Our findings might be used in the future for exploring clinical pain, given that sustained nociceptive stimuli more effectively simulate the dynamics of spontaneous pain in clinical conditions (Ploner and May 2018).

Acknowledgments

We wish to thank all members of our research group for their insightful comments on the manuscript.

Supplementary material

Supplementary material can be found at *Cerebral Cortex* online.

Funding

LH was supported by the National Natural Science Foundation of China (32071061 and 31822025). GDI was supported by an ERC Consolidator Grant (PAINSTRAT).

Conflict of interest statement. None declared.

References

Albe-Fessard D, Berkley KJ, Kruger L, Ralston HJ 3rd, Willis WD Jr. Diencephalic mechanisms of pain sensation. *Brain Res*. 1985:356(3):217–296.

Atlas LY, Lindquist MA, Bolger N, Wager TD. Brain mediators of the effects of noxious heat on pain. *Pain*. 2014:155(8):1632–1648.

Baumgartner U, Cruccu G, Iannetti GD, Treede RD. Laser guns and hot plates. *Pain*. 2005:116:1–3.

Baumgartner U, Greffrath W, Treede RD. Contact heat and cold, mechanical, electrical and chemical stimuli to elicit small fiber-evoked potentials: merits and limitations for basic science and clinical use. *Neurophysiol Clin*. 2012:42(5):267–280.

Benjamini Y, Hochberg Y. Controlling the false discovery rate: a practical and powerful approach to multiple testing. *J R Stat Soc B Methodol*. 1995:57:289–300.

Bruns A, Eckhorn R. Task-related coupling from high- to low-frequency signals among visual cortical areas in human subdural recordings. *Int J Psychophysiol*. 2004:51(2):97–116.

Colon E, Liberati G, Mouraux A. EEG frequency tagging using ultra-slow periodic heat stimulation of the skin reveals cortical activity specifically related to C fiber thermonociceptors. *NeuroImage*. 2017:146:266–274.

Corbetta M, Shulman GL. Control of goal-directed and stimulus-driven attention in the brain. *Nat Rev Neurosci*. 2002:3(3):201–215.

De Schoenmacker I, Berry C, Blouin JS, Rosner J, Hubli M, Jutzeler CR, Kramer JLK. An intensity matched comparison of laser- and contact heat evoked potentials. *Sci Rep*. 2021:11(1):6861.

Delorme A, Makeig S. EEGLAB: an open source toolbox for analysis of single-trial EEG dynamics including independent component analysis. *J Neurosci Methods*. 2004:134(1):9–21.

Dong WK, Chudler EH, Sugiyama K, Roberts VJ, Hayashi T. Somatosensory, multisensory, and task-related neurons in cortical area 7b (pf) of unanesthetized monkeys. *J Neurophysiol*. 1994:72(2):542–564.

Downar J, Crawley AP, Mikulis DJ, Davis KD. A multimodal cortical network for the detection of changes in the sensory environment. *Nat Neurosci*. 2000:3(3):277–283.

Garcia-Larrea L, Frot M, Valeriani M. Brain generators of laser-evoked potentials: from dipoles to functional significance. *Neurophysiol Clin*. 2003:33(6):279–292.

Gross J, Kujala J, Hamalainen M, Timmermann L, Schnitzler A, Salmelin R. Dynamic imaging of coherent sources: studying neural interactions in the human brain. *Proc Natl Acad Sci U S A*. 2001:98(2):694–699.

Guo Y, Bufacchi RJ, Novembre G, Kilintari M, Moayedi M, Hu L, Iannetti GD. Ultralow-frequency neural entrainment to pain. *PLoS Biol*. 2020:18(4):e3000491.

Hamalainen JA, Ortiz-Mantilla S, Benasich AA. Source localization of event-related potentials to pitch change mapped onto age-appropriate MRIs at 6 months of age. *NeuroImage*. 2011:54(3):1910–1918.

Hoechstetter K, Berg P, Scherg M. BESA research tutorial 4: distributed source imaging. *BESA Res Tutorial*. 2010:1–29.

Hu L, Iannetti GD. Neural indicators of perceptual variability of pain across species. *Proc Natl Acad Sci U S A*. 2019:116(5):1782–1791.

Hu L, Zhang Z. *EEG signal processing and feature extraction*: Singapore: Springer. 2019.

Hu L, Peng W, Valentini E, Zhang Z, Hu Y. Functional features of nociceptive-induced suppression of alpha band electroencephalographic oscillations. *J Pain*. 2013:14:89–99.

Hu L, Cai MM, Xiao P, Luo F, Iannetti GD. Human brain responses to concomitant stimulation of Aδ and C nociceptors. *J Neurosci*. 2014:34(34):11439.

Hu L, Valentini E, Zhang ZG, Liang M, Iannetti GD. The primary somatosensory cortex contributes to the latest part of the cortical response elicited by nociceptive somatosensory stimuli in humans. *NeuroImage*. 2014:84:383–393.

Hu L, Xiao P, Zhang ZG, Mouraux A, Iannetti GD. Single-trial time–frequency analysis of electrocortical signals: baseline correction and beyond. *NeuroImage*. 2014:84:876–887.

Iannetti GD, Mouraux A. From the neuromatrix to the pain matrix (and back). *Exp Brain Res*. 2010:205(1):1–12.

Iannetti GD, Hughes NP, Lee MC, Mouraux A. Determinants of laser-evoked EEG responses: pain perception or stimulus saliency? *J Neurophysiol*. 2008:100(2):815–828.

Jeon Y, Nam CS, Kim YJ, Whang MC. Event-related (De)synchronization (ERD/ERS) during motor imagery tasks: implications for brain-computer interfaces. *Int J Ind Ergon*. 2011:41(5):428–436.

Jonmohamadi Y, Poudel G, Innes C, Weiss D, Krueger R, Jones R. Comparison of beamformers for EEG source signal reconstruction. *Biomed Signal Process Control*. 2014:14:175–188.

Kayser C, Petkov CI, Lippert M, Logothetis NK. Mechanisms for allocating auditory attention: an auditory saliency map. *Curr Biol*. 2005:15(21):1943–1947.

Kurimoto R, Ishii R, Canuet L, Ikezawa K, Azechi M, Iwase M, Yoshida T, Kazui H, Yoshimine T, Takeda M. Event-related synchronization of alpha activity in early Alzheimer's disease and mild cognitive impairment: an MEG study combining beamformer and group comparison. *Neurosci Lett*. 2008:443(2):86–89.

Legrain V, Iannetti GD, Plaghki L, Mouraux A. The pain matrix reloaded: a salience detection system for the body. *Prog Neurobiol*. 2011:93(1):111–124.

Liberati G, Algoet M, Santos SF, Ribeiro-Vaz JG, Raftopoulos C, Mouraux A. Tonic thermonociceptive stimulation selectively modulates ongoing neural oscillations in the human posterior insula: evidence from intracerebral EEG. *NeuroImage*. 2019:188:70–83.

Magerl W, Treede RD. Heat-evoked vasodilatation in human hairy skin: axon reflexes due to low-level activity of nociceptive afferents. *J Physiol-London*. 1996:497(3):837–848.

Michel CM, Murray MM, Lantz G, Gonzalez S, Spinelli L, Grave de Peralta R. EEG source imaging. *Clin Neurophysiol*. 2004:115(10):2195–2222.

Moayedi M, Liang M, Sim AL, Hu L, Haggard P, Iannetti GD. Laser-evoked vertex potentials predict defensive motor actions. *Cereb Cortex*. 2015:25(12):4789–4798.

Mouraux A, Iannetti GD. Nociceptive laser-evoked brain potentials do not reflect nociceptive-specific neural activity. *J Neurophysiol*. 2009:101(6):3258–3269.

Mouraux A, Iannetti GD. The search for pain biomarkers in the human brain. *Brain*. 2018:141:3290–3307.

Mouraux A, Guerit JM, Plaghki L. Non-phase locked electroencephalogram (EEG) responses to CO2 laser skin stimulations may reflect central interactions between a partial partial differential- and C-fibre afferent volleys. *Clin Neurophysiol*. 2003:114(4):710–722.

Mulders D, de Bodt C, Lejeune N, Courtin A, Liberati G, Verleysen M, Mouraux A. Dynamics of the perception and EEG signals triggered by tonic warm and cool stimulation. *PLoS One*. 2020:15(4):e0231698.

Nickel MM, May ES, Tiemann L, Schmidt P, Postorino M, Dinh ST, Gross J, Ploner M. Brain oscillations differentially encode noxious stimulus intensity and pain intensity. *NeuroImage*. 2017:148:141–147.

Nickel MM, Ta Dinh S, May ES, Tiemann L, Hohn VD, Gross J, Ploner M. Neural oscillations and connectivity characterizing the state of tonic experimental pain in humans. *Hum Brain Mapp*. 2020:41(1):17–29.

Nir RR, Sinai A, Moont R, Harari E, Yarnitsky D. Tonic pain and continuous EEG: prediction of subjective pain perception by alpha-1 power during stimulation and at rest. *Clin Neurophysiol*. 2012:123(3):605–612.

Nunes AS, Moiseev A, Kozhemiako N, Cheung T, Ribary U, Doesburg SM. Multiple constrained minimum variance beamformer (MCMV) performance in connectivity analyses. *NeuroImage*. 2020:208:116386.

Onslow ACE, Bogacz R, Jones MW. Quantifying phase-amplitude coupling in neuronal network oscillations. *Prog Biophys Mol Biol*. 2011:105(1–2):49–57.

Palva S, Palva JM. Roles of brain criticality and multiscale oscillations in temporal predictions for sensorimotor processing. *Trends Neurosci*. 2018:41(10):729–743.

Panzeri S, Brunel N, Logothetis NK, Kayser C. Sensory neural codes using multiplexed temporal scales. *Trends Neurosci*. 2010:33(3):111–120.

Pascual-Marqui RD, Michel CM, Lehmann D. Low resolution electromagnetic tomography: a new method for localizing electrical activity in the brain. *Int J Psychophysiol*. 1994:18(1):49–65.

Peng WW, Hu L, Zhang ZG, Hu Y. Changes of spontaneous oscillatory activity to tonic heat pain. *PLoS One*. 2014:9(3):e91052.

Pfurtscheller G, Lopes da Silva FH. Event-related EEG/MEG synchronization and desynchronization: basic principles. *Clin Neurophysiol*. 1999:110(11):1842–1857.

Ploner M, May ES. Electroencephalography and magnetoencephalography in pain research-current state and future perspectives. *Pain*. 2018:159(2):206–211.

Ploner M, Sorg C, Gross J. Brain rhythms of pain. *Trends Cogn Sci*. 2017:21(2):100–110.

Purdon PL, Pierce ET, Mukamel EA, Prerau MJ, Walsh JL, Wong KFK, Salazar-Gomez AF, Harrell PG, Sampson AL, Cimenser A, et al. Electroencephalogram signatures of loss and recovery of consciousness from propofol. *Proc Natl Acad Sci U S A*. 2013:110(12):E1142–E1151.

Romei V, Brodbeck V, Michel C, Amedi A, Pascual-Leone A, Thut G. Spontaneous fluctuations in posterior alpha-band EEG activity reflect variability in excitability of human visual areas. *Cereb Cortex*. 2008:18:2010–2018.

Schulz E, May ES, Postorino M, Tiemann L, Nickel MM, Witkovsky V, Schmidt P, Gross J, Ploner M. Prefrontal gamma oscillations encode tonic pain in humans. *Cereb Cortex*. 2015:25(11):4407–4414.

Somervail R, Zhang F, Novembre G, Bufacchi RJ, Guo Y, Crepaldi M, Hu L, Iannetti GD. Waves of change: brain sensitivity to differential, not absolute, stimulus intensity is conserved across humans and rats. *Cereb Cortex*. 2021:31(2):949–960.

Tiemann L, Hohn VD, Ta Dinh S, May ES, Nickel MM, Gross J, Ploner M. Distinct patterns of brain activity mediate perceptual and motor and autonomic responses to noxious stimuli. *Nat Commun*. 2018:9(1):4487.

Tillman DB, Treede RD, Meyer RA, Campbell JN. Response of C fibre nociceptors in the anaesthetized monkey to heat stimuli: correlation with pain threshold in humans. *J Physiol*. 1995:485 (Pt 3):767–774.

Tracey I, Mantyh PW. The cerebral signature and its modulation for pain perception. *Neuron*. 2007:55(3):377–391.

Treede RD, Kenshalo DR, Gracely RH, Jones AKP. The cortical representation of pain. *Pain*. 1999:79(2–3):105–111.

Treede RD, Lorenz J, Baumgartner U. Clinical usefulness of laser-evoked potentials. *Neurophysiol Clin*. 2003:33(6):303–314.

Vanneste S, Song JJ, De Ridder D. Thalamocortical dysrhythmia detected by machine learning. *Nat Commun*. 2018:9(1):1103.

Wager TD, Davidson ML, Hughes BL, Lindquist MA, Ochsner KN. Prefrontal-subcortical pathways mediating successful emotion regulation. *Neuron*. 2008:59(6):1037–1050.

Werner S, Noppeney U. The contributions of transient and sustained response codes to audiovisual integration. *Cereb Cortex*. 2011:21(4):920–931.

Woo CW, Roy M, Buhle JT, Wager TD. Distinct brain systems mediate the effects of nociceptive input and self-regulation on pain. *PLoS Biol*. 2015:13(1):e1002036.

Zhang CH, Sohrabpour A, Lu YF, He B. Spectral and spatial changes of brain rhythmic activity in response to the sustained thermal pain stimulation. *Hum Brain Mapp*. 2016:37(8):2976–2991.